Experimental Mechanics (2016) 56:1351–1362
DOI 10.1007/s11340-016-0169-7

Experimental Investigation of Plastic Strain Recovery and Creep in Nanocrystalline Copper Thin Films

N. Ghazi[1] · J. W. Kysar[1]

Received: 6 February 2016 / Accepted: 9 May 2016 / Published online: 26 May 2016

Abstract Nanocrystalline metals exhibit a phenomenon called plastic strain recovery whereby plastic strain introduced through a load cycle is gradually recovered under no external loading over a time period of hours and days. In this study, we experimentally explore the diffusive mechanisms and the strain rates for nanocrystalline thin films of copper with an average grain size of about 35 nm during plastic strain recovery and creep. The experiments are performed via the plane strain bulge test and the thin film samples are deposited using thermal evaporation and sputtering. The specimens recover their residual strain in a period of time with two characteristic strain rates, a transient strain recovery rate of the order of $10^{-7}/s$ and a steady-state strain recovery rate of the order of $10^{-9}/s$ and there is a characteristic time at which the transition occurs between the two rates. The results suggest that a diffusive mechanism in conjunction with voids within the nanocrystalline material can explain the two plastic strain recovery rates and the transition between the two.

Keywords Nanocrystalline thin film · Grain boundary diffusion · Plastic strain recovery · Creep · Thin film bulge test

✉ N. Ghazi
nng2107@columbia.edu

[1] Department of Mechanical Engineering, Columbia University, 500 West 120th Street, New York, NY 10027, USA

Introduction

Nanocrystalline thin metal films are defined as thin films with an average grain size of less than 100nm. These films have been the subject of widespread research in recent years due to their enhanced material properties and behavior compared to their coarse-grain counterparts, such as higher yield and fracture strength, decreased elongation and toughness and strain rate sensitivity [1–6].

Nanocrystalline metals exhibit a phenomenon called plastic strain recovery whereby plastic strain introduced through a load cycle is gradually recovered (i.e. reversed) under no external loading over a time period of hours and days [7, 8]. Energy is dissipated in the load cycle, so the process is not reversible in a thermodynamic sense. The creation, motion and multiplication of dislocations is the dominant deformation mechanism in microcrystalline materials. However, when the grain size is reduced to the nanometer scale, dislocation sources and activities are highly constrained by the small volumes. Thus, nanocrystalline metals can achieve significantly higher stresses than their microcrystalline counterparts. Given the high stresses coupled with the high volume fraction of grain boundaries in nanocrystalline metals, inelastic deformation in nanocrystalline metals is often dominated by grain boundary deformation mechanisms [9]. These mechanisms included grain boundary diffusion and grain boundary sliding [10–12]. Creep deformation in nanocrystalline metals is a consequence of grain boundary diffusion[13]. , In addition, the inverse Hall-Petch effect [14–16] and strain rate sensitivity [17, 18] observed in nanocrystalline metals, but not typically observed in microcrystalline metals, are the result of grain boundary deformation mechanisms.

Plastic strain recovery occurs at very small rates of $10^{-9}s^{-1}$ to $10^{-7}s^{-1}$ which suggests that diffusive mechanisms play a key role in the phenomenon [7, 10]. In this paper we experimentally explore the diffusive mechanisms and the strain rates for nanocrystalline thin film of copper during plastic recovery and creep in free-standing thin films. The experiments are performed via the plane strain thin film bulge test. The experiments measure elastic modulus, monitor plastic strain recovery and the strain rate during creep. We demonstrate that there are two characteristic plastic strain recovery rates and a characteristic time at which a transition occurs between the two rates. We also discuss briefly the results of a detailed numerical simulation of the load cycle and plastic strain recovery in nanocrystalline metals. The results suggest that a diffusive mechanism in conjunction with voids within the nanocrystalline material can explain the two plastic strain recovery rates as well as the transition between the two.

Experimental Methods for Nanocrystalline Thin Films

Mechanical properties of microscale metal thin films can vary considerably from their bulk counterparts [19]. Several specialized techniques have been developed to characterize the mechanical behavior of thin films including nanoindentation, microbeam bending, microtensile testing, bulge testing, x-ray diffraction, and substrate curvature measurement [20]. Elastic, plastic, creep, fatigue, fracture toughness, interfacial toughness as well tribological properties can be determined utilizing these techniques, however each of these methods has drawbacks in determining some of the material properties. For nanoindentation, with relative simple fabrication and preparation, the main drawback is that the stress state beneath the indentation is complex [21–24]. Likewise, microbending [25, 26] has relatively simple fabrication with the drawback that the film strain can only be changed by changing the temperature, thus making it difficult to interpret the results [27]. The methods above use samples on substrates. To measure the mechanical behavior of free-standing thin films, the micro-tensile test and the bulge test techniques are widely used. These techniques require more sample preparation, but they can be readily applied to measure film properties without any substrate effects and to characterize thin film constitutive behavior with relatively large applied strains [28]. In uniaxial tensile testing of thin films, three issues need to be considered: specimen preparation, force application, and strain measurement [29]. The difficulty is to measure accurately the strain so that the Young's modulus can be determined [30]. In the bulge test, free-standing thin films are obtained by opening a window from the backside in the substrate. The free-standing film is deflected by applying a uniform pressure to the film. The mechanical properties of the film are determined from its pressure-deflection behavior. Compared with microtensile testing, the bulge test technique has the unique advantage of precise sample fabrication and minimal sample handling. The other major advantages associated with bulge test are the ability of imposing unambiguous loading conditions, applicability at wafer level and allowing measurement of the residual stress in the material. Therefore, it is not surprising that the bulge test method has many applications in the field of materials testing such as dynamic mechanical loading, creep and viscoelastic, and high-temperature tests [28, 31–40]. In this study, the bulge test method is used to investigate the time dependent elastic-plastic response of nanocrystalline thin metal films for strain rates as low as $10^{-6} - 10^{-7}s^{-1}$ where the role of grain boundary diffusion mechanism in deformation becomes significant. This method can be performed under constant strain rate to avoid the effect of strain rate sensitivity especially for nanocrystalline thin films which have higher strain rate sensitivity [28, 41]. In addition, the method is amenable to the measurement of the plastic strain recovery rate at very slow rates for long periods of time.

Introduction to the Plane-Strain Bulge Test Technique

To explain the experimental data and relate them to mechanical properties of the tested films, both theoretical and numerical analyses have been conducted to understand the pressure–deflection relation for membranes with various shapes of free standing thin films [37, 42–46]. Vlassak and Nix derived an expression for the elastic load–deflection behavior of square and rectangular membranes following an approach originally developed by Timoshenko [46] while accounting for residual stress in the membrane. These researchers further found that once the aspect ratio of a rectangular membrane exceeds four, the deflection at the center of the membrane is nearly independent of the aspect ratio and can be approximated with the exact plane strain solution for an infinitely long rectangular membrane, which can be readily derived [37].

The accuracy and reliability of the bulge test has been analyzed by a number of researchers. Vlassak [43] investigated the contribution of the film bending stiffness to the deflection of a membrane. He showed that for typical bulge test geometries, the bending moment is only significant very close to the edge of the membrane and is negligible everywhere else. These analyses, together with new sample preparation techniques based on Si micromachining, revolutionized the bulge test to be a useful technique to accurately measure the elastic properties of both freestanding films

and multilayers across a wide range of materials, including ceramics, metals, polymers [37, 39, 47]. Because the bulge test technique measures isothermal stress-strain curves of freestanding films, it is also ideal for studying plasticity in thin films.

Sample Preparation and Characterization

Free standing thin copper films are fabricated using standard procedures [38]. Briefly, a silicon wafer (⟨100⟩ surface orientation) with both sides coated with 100nm low pressure chemical vapor deposition (LPCVD) silicon nitride is used as the substrate. In Fig. 1 a schematic of the bulge test sample preparation is shown. The wafer is anisotropically back etched in KOH through its thickness to obtain a free standing thin film of silicon nitride that spans the etched cavity. At the final step a thin layer of nanocrystalline metal is deposited on atop the silicon nitride using either thermal evaporation or sputter deposition after which the silicon nitride beneath the metal film is removed via reactive ion etching.

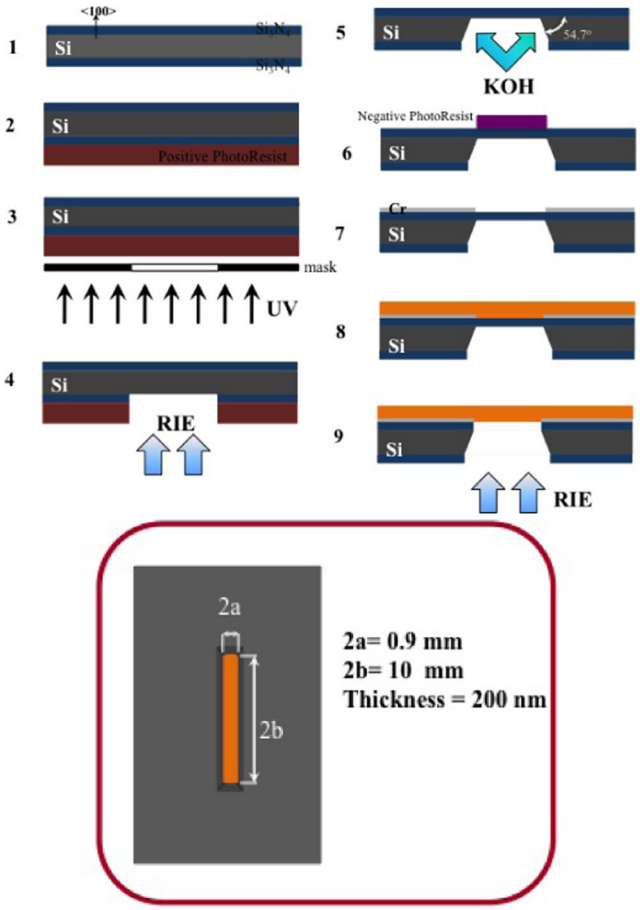

Fig. 1 Free-standing film fabrication steps: 1)⟨100⟩ silicon wafer coated with LPCVD silicon nitride on both sides, 2) and 3) standard photolithography to pattern a window on the rear silicon nitride surface, 4) reactive ion etching to etch the patterned window through silicon nitride, 5) anisotropic wet etching of silicon to open etch cavity, 6) coating the freestanding silicon nitride with negative photoresist , 7) depositing adhesion layer and lift it up from the free-standing film, 8) depositing copper, 9) reactive ion etching to remove silicon nitride beneath the copper

For both the thermal evaporation and sputter deposition methods, used in this work, the deposition thickness is below 1μm and the deposition time is less than 2 hours. During deposition, the substrate temperature (T_s) in maintained much below the metal melting temperature (T_m) of copper to obtain a microstructure with so-called Zone 1 behavior [48, 49]. These conditions lead to a very slow surface diffusion and the lack of bulk self-diffusion, so the resulting film consists of small tapered crystals with domed tops separated by void boundaries and the internal grains usually have a high dislocation density.

To measure the thickness of the deposited film we used a DekTak 3 Stylus Profilometer. To characterize the grain size, X-ray diffraction is performed (Inel XRD 3000 module, CuK_α). Scherrer derived a formula to express the relation between the grain size and full width at half maximum (FWHM) of the Bragg angle peak [50]. Williamson and Hall [51] used Scherrer's theory to make a standard tool for investigation the grain size which we employed to characterize the average grain size of the copper films.

According to Williamson-Hall, the value for Full Width at Half Maximum (FWHM) denoted β is given approximately as [51–53]:

$$\beta = 4\varepsilon tan\theta + K\lambda/Dcos\theta \tag{1}$$

where θ is the Bragg angle, and ε is the integral breath of lattice strain distribution induced in the nanocrystals due to imperfection and distortion, D, K and λ are correspondingly the average dimension of crystallites, unit cell geometry dependent constant and X-ray wavelength. Upon rewriting equation (1) as

$$\beta cos(\theta) = 4\varepsilon sin(\theta) + K\lambda/D \tag{2}$$

the slope of the plot of $\beta cos(\theta)/\lambda$ versus $sin(\theta)/\lambda$ gives information about the ε and D and the intercept gives the inverse of the averaged grain size.

A typical X-ray diffraction pattern for 200 nm thick copper film deposited by thermal evaporation is shown in Fig. 2a. This pattern contains four Bragg peaks of (111), (200), (220) and (311) plane orientations. To find the FWHM at each peak we used the Pseudo-Voigt function [54]. Figure 2b shows each peak in the Williamson-Hall line with $\beta cos(\theta)/\lambda$ as as the abscissa and $sin(\theta)/\lambda$ as the ordinate.

The intercept in the plot is $K/D = 0.0048$ where $\lambda = 1.57$ Å. This gives a grain size of around $35\,nm$.

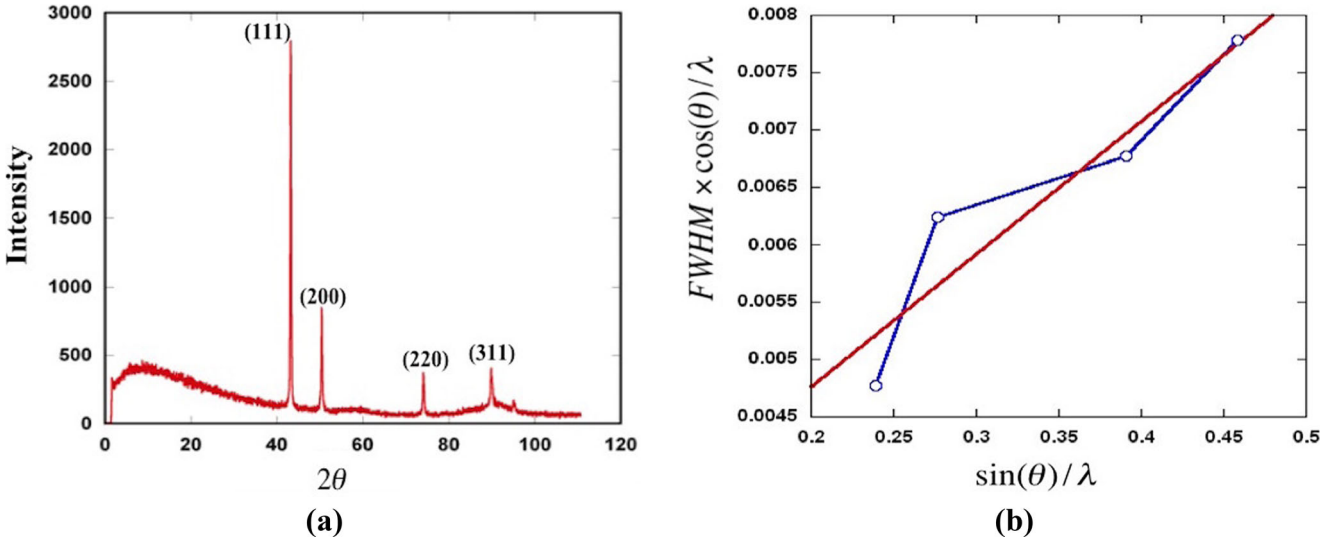

Fig. 2 (**a**) X-ray diffraction pattern for 200 nm thin film, (**b**) Williamson-Hall plot from X-ray diffraction pattern of the film

We also analyzed the samples using Scanning Electron Microscope (SEM) as in Fig. 3 which shows the grain structure on the surface of the thin film for both deposition methods. The grain size in the films is characterized by line intercept method [55] to obtain grain sizes of films deposited by thermal evaporation and sputtering of $35\,nm$ and $36\,nm$, respectively. However by comparing the SEM images of sputtering and thermal evaporated samples it can be seen that the porosity between grains is more noticeable and density of cracks and voids are increased in sputtered films. The consequence of that on the results is discussed later in this paper.

Plane Strain Bulge Test Setup

The bulge test method is a technique by which a uniform (e.g. air) pressure is applied on the thin film to induce stress. As a result the thin film membrane deflects and causes a distributed strain to develop within the film as shown schematically in Fig. 4a. The air pressure is applied from the backside and is controlled by an electrical pressure regulator (Bellofram Inc.) with accuracy of $0.2kPa$. The applied pressure is measured with a pressure transducer (Kulite XTEL-190(M) series). The pressure regulator and pressure transducer output are collected with a data acquisition card (DAQ PCI-6024E) via data acquisition modules. A LabView program (National Instrument) is designed to control the pressure inside the chamber to define loading and unloading loops with desired rates. A scanning laser confocal profilometer (LT-9100, Keyence Inc.) is used to measure the out-of-plane deformation profile at a cross-section of the thin film. The out-of-plane deflection data are simultaneously collected with the pressure data.

To find an approximate relation between stress and strain in the sample based on the two measured data (pressure and out-of-plane deformation in the cross-section), we use the approach and assumptions proposed by Vlassak and Nix

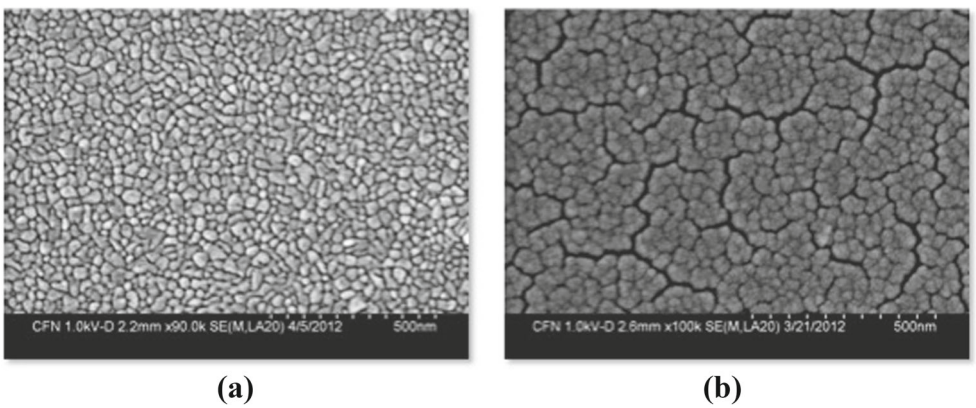

Fig. 3 SEM images of the thin film with thickness of 200 nm: (**a**) thermal evaporation, (**b**) sputtering

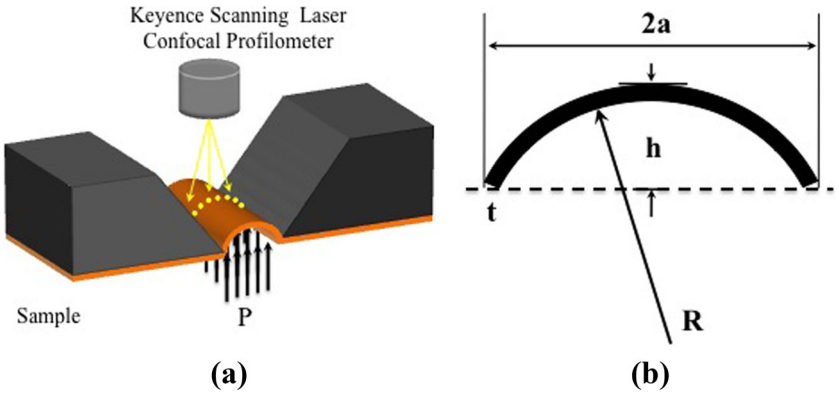

Fig. 4 (**a**) Schematic of plane strain bulge test. (**b**) Cross-section of the membrane during deformation

[35, 43]. Briefly, the contribution of bending to the strain energy is neglected ($EI \rightarrow 0$ where E is the elastic modulus and I is the moment of inertia) and the edge of freestanding film can be treated as plastic hinges. This is valid because the deflection h is much larger than the thickness of the film as shown schematically in Fig. 4b.

For a rectangular membrane with the aspect ratio of length to the width of film more than four, plane-strain conditions hold and the cross-section adopts a cylindrical profile [28].

The stress and strain are then uniform across the width of the membrane independent of whether the film deforms elastically or plastically, and are given by:

$$\sigma = \frac{P(a^2+h^2)}{2ht} = \frac{PR}{t} \tag{3}$$

$$\varepsilon = \frac{a^2+h^2}{2ah}\arcsin\left(\frac{2ah}{a^2+h^2}\right) - 1 = \frac{R}{a}\arcsin\left(\frac{a}{R}\right) - 1 \tag{4}$$

where P is the pressure applied on the film, R is the radius of the curvature of the deformed film, t is the film thickness and a is one-half of the film width and h is the deflection at the center of the film.

The measured experimental parameters (pressure & out-of-plane deflection profile) will be used in equations (3) and (4) to calculate stress and strain independently to characterize the material properties of thin films.

Results and Discussion

In the bulge test experiment the pressure, P, is gradually increased during the loading portion of load cycle which results in deflection of the film into a cylindrical cross-section with radius of curvature R. By increasing the pressure, the radius R is decreased and the out-of-plane deformation is increased. We measure the film cross-section profile with the laser scanning profilometer. The value of R is determined by fitting the measured out-of-plane deformation profile at a cross-section to the equation of a circle. In Fig. 5, blue lines show the film curvature at each discrete times and red lines represent fitted circles to find the curvature when the film is pressurized. Also when the membrane is unpressurized gradually (unloading part of the load cycle), the radius of the curvature increases and out-of-plane decreases.

In this work, three sets of bulge test experiments are performed on the nanocrystalline thin film. The first was to measure the elastic properties of the films. The second was the characterize the plastic strain recovery rate. The third was to measure the creep properties of the nanocrystalline thin films.

Young's Modulus

To measure the Young modulus (E) of thin copper film, the membrane is pressurized gradually during the first loading step. After reaching the desired stress, the unloading step is performed and the pressure on the film is reduced with the same rate as in loading to reach to zero pressure. The loading strain rate is of the order of $10^{-6}/s$ for this

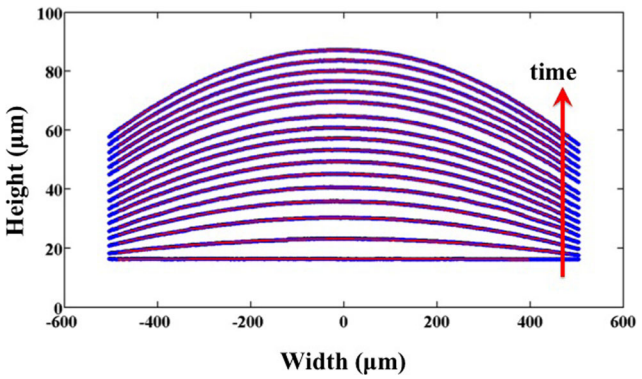

Fig. 5 Cross-section of the film profile with time

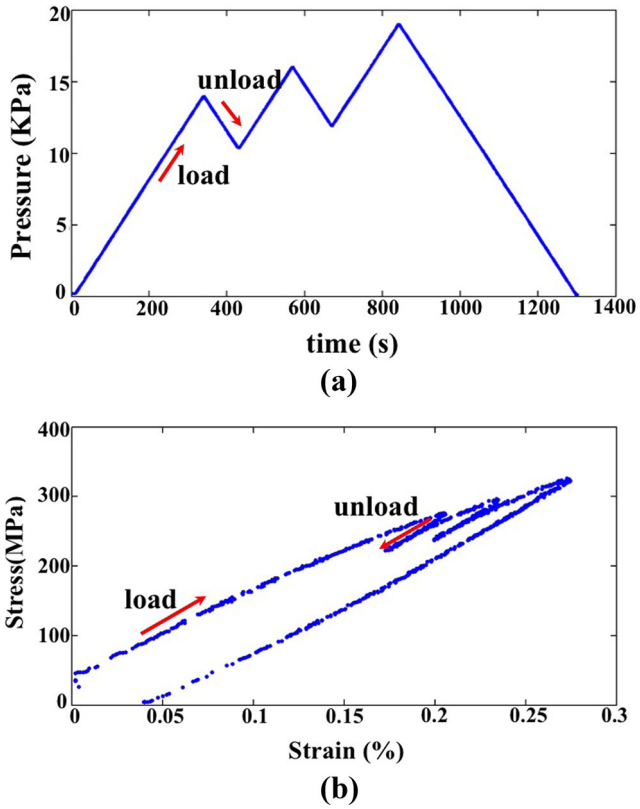

Fig. 6 (**a**) Pressure-time and (**b**) resulting stress-strain curves

experiment. From the unloading slope on the stress-strain curve, the plane-strain modulus, M, can be obtained; subsequently, the Young's modulus of the material is determined as $E = (1 - \nu^2)M$, where ν is the Poisson's ratio; taken to be 0.35 as the value for bulk copper [56]. The loading-unloading cycle is done several times and the modulus is averaged; see Fig. 6. The experimental results are shown in Table 1 for samples deposited with thermal evaporation and Table 2 for samples deposited with sputtering.

The Young's modulus for 38 thin film samples with thicknesses in the range of 195 nm to 270 nm was measured to be in the range of $100 - 157\ GPa$ (1). This is in good agreement with published values for bulk materials which is in the range between 109 GPa to 144 GPa [56]. The values obtained for Young modulus, are based on assumptions of isotropic and homogeneous material properties and uniform thickness. The non-ideal fabrication process may introduce inhomogeneities and thickness variations that likely lead to the observed scatter in elastic modulus. However for nanocrystalline thin films deposited with sputtering, the measured stiffness is below the stiffness reported for bulk materials. This can be explained due to increased density of cracks and voids in the sputter deposited thin film, that results in having a less dense material relative to the polycrystalline one. Comparing the SEM image of sputtering and thermal evaporated samples also confirms this hypothesis, since the porosity between grains is more noticeable in sputtered films [57].

Plastic Strain Recovery

For conventional plastically deformed materials with grain size of the order of microns, plastic deformation is typically irreversible. When a material yields, plastic strain remains in the material permanently if no external work is done on the material. Plasticity in microcrystalline metals is known to be due to dislocation activities. Dislocations are very stable so to remove them requires significant external energy, such as that supplied while annealing at high temperature .

However, plastic deformation in nanocrystalline materials is found to be partially to fully recoverable at room temperature with no external tractions. Such plastic strain recovery has been reported in two other studies [7, 8]. In both studies free-standing thin films of a FCC metal with grain sizes less than 100 nm are tested at room temperature. In one, a microtensile test with strain rate of $10^{-4}/s$ is performed [8]and partial recovery is observed after complete unloading at room temperature. In the other study, a plane strain bulge test with strain rate of $5 \times 10^{-5}/s$ is applied [7] and plastic strain is fully recovered after unloading.

In this paper, we further explore the plastic strain recovery rates for copper thin film samples deposited via both thermal evaporation and sputtering and also for bulge tests performed at two different strain rate for both loading and unloading. In these experiments the membrane is pressurized gradually with a loading strain rate of $10^{-6}/s$ or $10^{-7}/s$ to develop plastic strain to about 0.5% strain in the

Table 1 Young's modulus for samples deposited with thermal evaporation

Film thickness (nm)	Number of samples	AverageYoung's Modulus (GPa)	Standard deviation (GPa)
195	7	133	22
200	5	130	25
215	4	157	29
220	7	137	40
240	4	105	26
260	7	101	8
270	4	115	22

Table 2 Young's modulus for samples deposited with sputtering

Film thickness (nm)	Number of samples	AverageYoung Modulus (GPa)	Standard Deviation (GPa)
185	11	64	9

membrane under plane strain conditions. Unloading occurs immediately after loading by decreasing the pressure with exactly the same rate as loading to remove external pressure from the membrane. The specimen—having lengthened via inelastic deformation during the loading phase—buckles and develops wrinkled after the pressure is removed completely [7]. The plastic strain recovery is visible to the naked eye as the amplitude of the wrinkles gradually reduces over the period of several days until the film is flat and taut over the window in the substrate. To quantify the rate of plastic strain recovery, we measure the cross-section profile of the wrinkled film as a function of time using the laser scanning profilometer. The length of the cross-section of the free-standing film is determined by numerical integration of the scanned sectional coordinates of the profile at intervals of $2\,\mu m$. The current value of inelastic strain at each moment is obtained based on the difference in initial cross-sectional length before loading and the length at the current time. It should be emphasized that in the buckled state the film is not under influence of any external tractions, other than the negligible stress due to the film bending. The plastic strain recovery results for nanocrystalline thin films of 200 nm thickness samples are shown in Table 3.

In all the specimens tested herein the plastic strain is fully recovered. The evolution of a representative cross-section of a thermally deposited 200nm thick copper film during recovery (tested at room temperature with a loading strain rate of 3×10^{-6}) is shown in Fig. 7. The film buckles into a higher mode rather than the first mode because of the constraints at the ends of the specimen (e.g. top and bottom specimen ends shown in Fig. 1).

Our experiments demonstrate that the recovery process for each loading cycle regardless of the loading rate and deposition method has a transient stage followed by a steady-state stage, as shown in Fig. 8. For the samples deposited with thermal evaporation and loaded with strain rate of about $10^{-6}/s$ the transient plastic strain recovery rate is in the order of $10^{-7}/s$. The steady-state strain recovery rate is of the order of $10^{-9}/s$. The transition from the transient to steady state plastic strain recovery rate occurs at about 2000s. When the loading and unloading rates are decreased by one order of magnitude, most of the transient strain recovery occurs during the unloading and the transient rate after complete unloading decreases to be of the order of $10^{-8}/s$, but the transition time to steady state and the steady state plastic strain recovery rate remains approximately the same.

For samples deposited with sputtering there are two transitions in the plastic strain recover rate. When loaded with a strain rate of $10^{-6}/s$, the plastic strain recovery initially starts sharply with a transient rate of $10^{-6}/s$ for about 300s followed a transition to another transient rate in the order of $10^{-7}/s$. After a total of about 2500s a steady state plastic strain recovery is achieved that is somewhat higher than the steady state rate in the thermally evaporated specimens. The summary of residual strain recovery rates and times are shown in Table 4.

Creep Test

To observe the film behavior under creep, the sample is pressurized to achieve a strain rate of the order $10^{-6}/s$ up to the point that the stress is around 400 MPa in the film. Then we control the pressure rate to maintain a prescribed constant stress in the membrane using the relation between stress σ, pressure P and curvature radius R in equation (3). To do so, we monitor the radius of the curvature continuously and change the pressure to maintain a constant PR. Figure 9a shows the total creep strain accrued at a constant stress throughout a representative experiment for thermal evaporation deposited $200\,nm$ nanocrystalline copper film. Figure 9b shows the strain versus time. Figure 9c shows the strain rate during the creep of the same sample. It is evident that the creep strain rate is higher at the beginning and

Table 3 Plastic strain recovery rate

Deposition method	Loading rate (s^{-1})	No. of samples	Film thickness (nm)	Transient strain recovery rate (s^{-1})	Transient duration (s)	Steady-state strain recovery rate (s^{-1})
Thermal evaporation	10^{-6}	6	195–270	$1 \sim 3 \times 10^{-7}$	2000	$2 \sim 4 \times 10^{-9}$
Thermal evaporation	10^{-7}	2	195–270	3×10^{-8}	2500	3×10^{-9}
Sputtering	10^{-6}	3	185	$10^{-6} - 3 \sim 9 \times 10^{-7}$	300–2500	$9 \times 10^{-8} - 5 \times 10^{-9}$

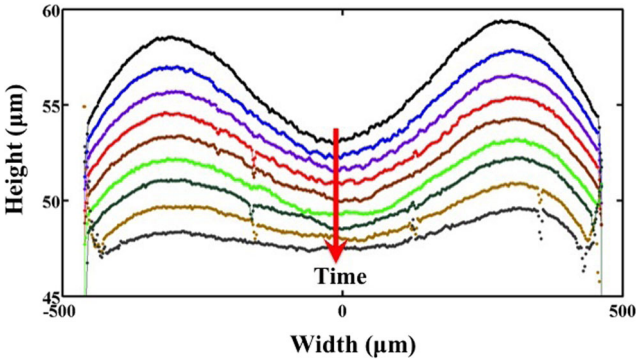

Fig. 7 The evolution of the cross-section profile during 30 hours after a load and unload cycle of $5 \times 10^{-6}/s$

gradually decreases by time. Nonetheless, the experimental values reported are the strain rate.

Table 4, shows the average value of creep strain rates on various samples. The creep strain rate for both deposition methods and temperatures at which the experiments are performed remains the same order of magnitude. The experimental value for the creep strain rate can be averaged at room temperature to be $\dot{\varepsilon} = 3.7 \times 10^{-7}/s$.

Coble [58] studied the relation between macroscopic creep strain $\dot{\varepsilon}$, applied tensile stress and the grain size of the materials by assuming the macroscopic shape change of crystals is due to diffusional transport of atoms along grain boundaries. The relationship for the creep behavior relating strain rate ($\dot{\varepsilon}$) during the creep to the applied stress (σ), grain size and temperature is

$$\dot{\varepsilon} = \alpha \frac{\delta_{gb} D_{gb} \Omega}{kT} \frac{\sigma}{d^3} \tag{5}$$

where α is a proportionality constant that depends on the grain shape, k is Boltzmann constant, T is temperature, Ω is atomic volume, d is the grain size and finally $\delta_{gb} D_{gb}$ is grain boundary diffusion coefficient multiplied by grain boundary thickness which is referred to as the diffusion flux in grain boundary for nanocrystalline materials. Equation (5) predicts a stress-strain rate relation during the creep and also emphasizes that Coble diffusional creep becomes an important role in the inelastic deformation in polycrystalline when the grain size decreases ($\dot{\varepsilon} \propto d^{-3}$). Although the typical homologous temperature for activating the Coble diffusion is of the order of $0.3T_m$ for bulk materials (where T_m is the absolute melting temperature) for nanocrystalline materials with average grain size less than $100\,nm$, Coble-type grain boundary diffusion is often the dominant deformation mechanism even at room temperature [59, 60].

Therefore equation (5) is valid for this case so the value for $\delta_{gb} D_{gb}$ can obtained. Following [10] we assume the value for α to be 1, which is two orders of magnitude smaller than the value suggested by Coble [58]. There are two reasons for this difference: first, Coble's result is based on a three-dimensional analysis of grains and second, the result assumes free grain boundary sliding. Adding viscosity to the grain boundary substantially reduces the rate of the creep and consequently α [10]. Further, it is also has been shown experimentally that the the diffusional creep at room temperature for nanocrystalline materials is two order of magnitudes smaller than the predicted value with Coble creep using $\alpha = 144$ [61]. Therefore we calculate the value of $\delta_{gb} D_{gb}$ to be $8.36 \times 10^{-30} m^3/s$ using the atomic volume $\Omega = 1.8 \times 10^{-29}\, m^3$, room temperature $T = 300\,\mathrm{K}$, Boltzmann constant $k = 1.38 \times 10^{-23} m^2 kg s^{-2} K^{-1}$. The value obtained for grain boundary diffusion is consistent with reported values for nanocrystalline materials obtained from numerical simulation [18].

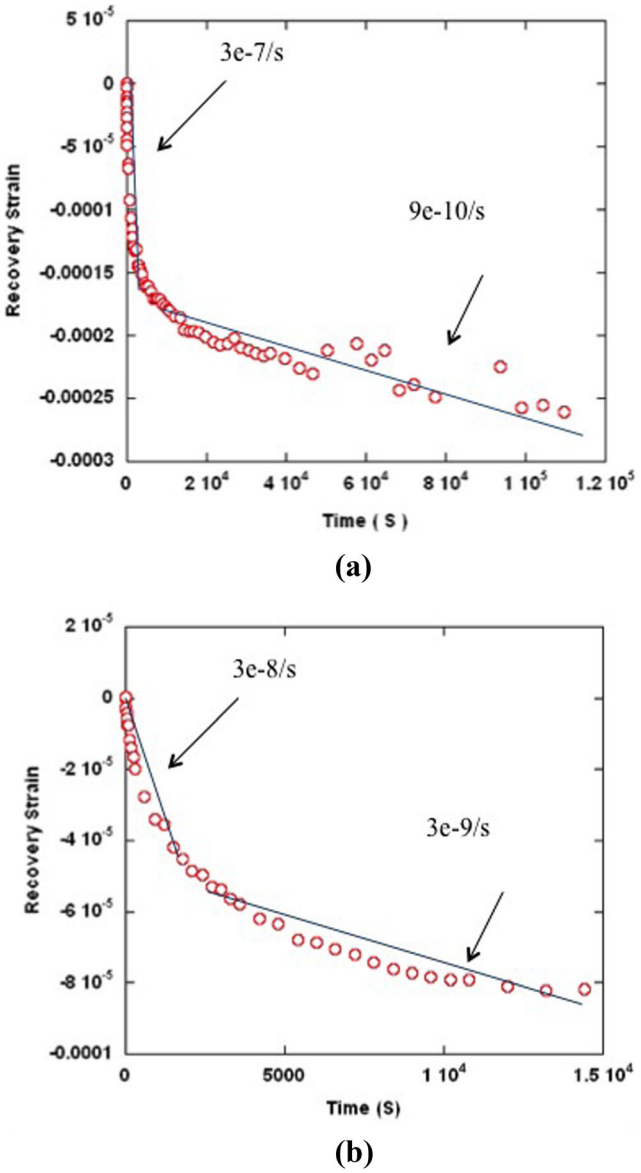

Fig. 8 Plastic strain recovery (**a**) loading rate $5 \times 10^{-6}/s$ (**b**) loading rate $5 \times 10^{-7}/s$

Table 4 Creep strain rate of nanocrystalline copper thin films

Deposition method	Temperature (K)	No. of samples	Thickness (nm)	Average initial creep rate (1/s)	Standard deviation (1/s)	Initial creep duration (sec)	Average secondary creep rate (1/s)	Standard deviation (1/s)
Thermal evaporation	room temp.	10	195-220	4.13×10^{-7}	2.18×10^{-7}	2000	5.54×10^{-8}	1.2×10^{-8}
Thermal evaporation	370	2	200	4.8×10^{-7}	8.9×10^{-8}	700		
Sputtering	room temp.	9	185-200	3.31×10^{-7}	1.18×10^{-7}	3000	4.28×10^{-8}	1.19×10^{-8}
Sputtering	370	2	185	8.35×10^{-7}	3.5×10^{-7}	500		

Thus the grain boundary diffusion mechanisms that lead to Coble creep can be considered to be dominant deformation mechanisms in our experiments.

Numerical Simulation

Grain boundary diffusion associated with Coble creep is the dominant deformation mechanism in nanocrystalline copper thin films under a homogeneous stress state induced by an external loading. Hence we assume that grain boundary diffusion will also be the dominant deformation mechanism during plastic strain recovery. However since no external traction is applied to the material during plastic strain recovery the process must be driven by residual stresses that induce gradients in chemical potential that drive the diffusive mechanisms. The presence of chemical potential gradients during plastic strain recovery requires that plastic deformation during the loading phase to have been heterogeneous. That, in turn, requires the material itself to be heterogeneous on a scale larger than the grain size. Nanocrystalline thin films are known [62] to contain voids on grain boundaries that have average sizes much smaller than the grain size and are separated by distances much

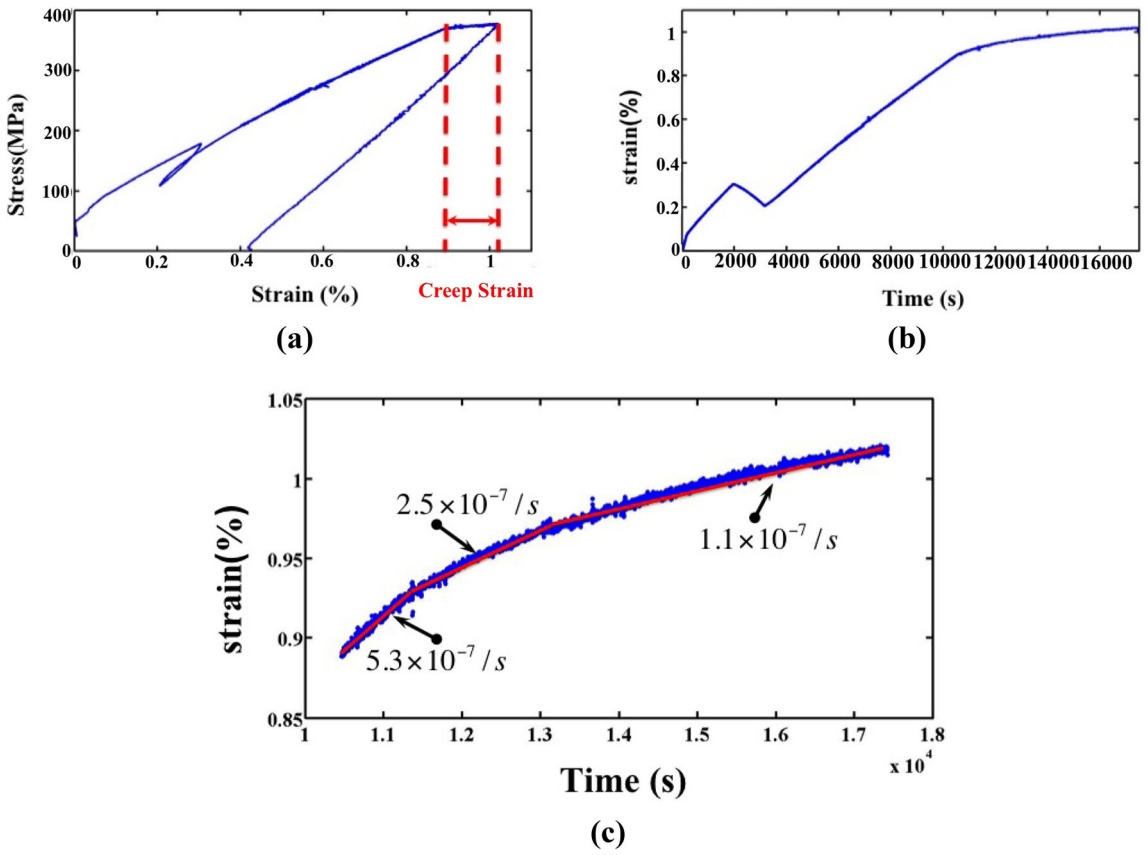

Fig. 9 (**a**) Stress-strain, (**b**) strain-time plot for creep test, and (**c**) creep strain rate

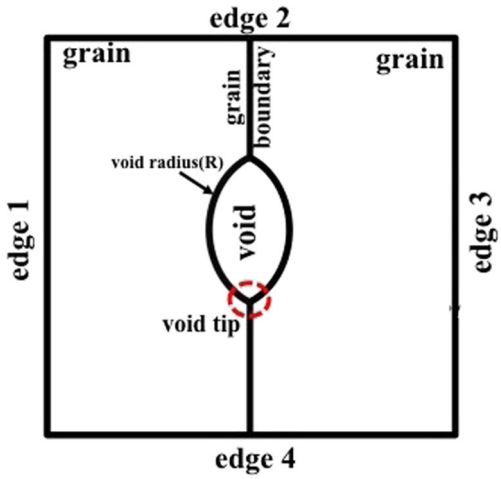

Fig. 10 Schematic of the numerical model

larger than the grain size. We postulate in the simulation that these voids play a key role in the phenomenon of plastic strain recovery.

We perform a detailed numerical simulation in which we model diffusion on grain boundaries and between grain boundaries and voids in nanocrystalline copper films. Herein we discuss the salient points of the simulation and its results; full details of the simulation will be published elsewhere. The computational domain used in the simulations, shown in Fig. 10, consists of a two dimensional (2D) assembly of grains and grain boundaries in accordance with plane strain assumption. The nanocrystalline model consists of two rectangular grains of the same size separated by a grain boundary. Diffusion within the grain boundary is assumed to occur within a "diffusion zone" of initial thickness of $1\,nm$. In addition, a pre-existing void is assumed to be in the middle of the grain boundary. Periodic boundary conditions (PBC) are applied on the edges of the model such that the displacement in the horizontal direction is constrained to be zero on edge 1 and the displacement in the vertical direction is constrained to be zero at edge 4. The displacements in the horizontal and vertical directions are also constrained to be uniform on edge 3 and 2 respectively. Consistent with the experiments, the system experiences a uniaxial tensile stress in the horizontal direction during the loading phase of the load cycle.

The material properties within both grains are the same and assumed to be isotropic and elastic-plastic. To account for grain boundary diffusion, we incorporate a diffusion zone (DZ) that coincides with the grain boundary. In addition on the same boundary, a cohesive zone (CZ) is defined to account for potential traction-separation behavior. Both the DZ and CZ models are formulated in a UEL (User Element) and implemented within the general purpose finite code ABAQUS. Diffusion is also modeled on the surface of the void as driven by chemical potential gradients due to curvature changes. Finally, diffusive flux at the void tip between the grain boundary and the void surface is driven by the jump in chemical potential. By formulating the driving forces for diffusion over the grain boundary and void surface as a mechanism for deformation, we determine the direction and magnitude of flux on the void surface as well as in the the grain boundary.

The results of the simulation indicate that the diffusive fluxes within the grain boundaries are highly heterogeneous. Specifically, there is a large tensile normal stress concentration on the grain boundary at the void tips during the loading phase. This drives diffusive flux toward the void tip from the remaining grain boundary as well as from the void surface to the grain boundary. As a consequence, there is a net atomic flux toward the void tip so that the average thickness of the "diffusion zone" increases which leads

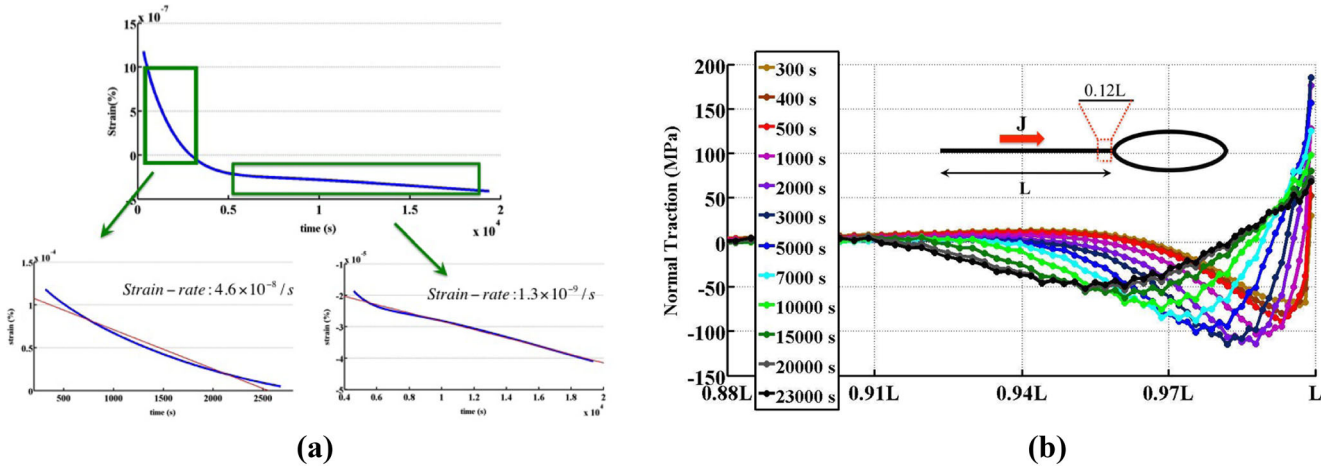

Fig. 11 (**a**) Plastic strain recovery rates obtained from numerical simulation, (**b**) normal tensile stress over the grain boundary

to an increase in length of the specimen that is observed experimentally as an overall inelastic strain on the specimen. During the unloading phase of the load cycle all eternal tractions are removed and the excess material in the grain boundary induces a compressive normal stress on the grain boundary near the void tip. In that way the chemical potential gradient is reversed which drives a net atomic flux away from the void tip on the grain boundaries as well as from the grain boundary to the void surface. This atomic flux from the grain boundary to the void surface leads to a net loss of material in the diffusion zone which leads to an decrease in length of the specimen that is observed experimentally as a recovery of the plastic strain. Initially the large chemical potential gradient due to the excess material near the void tip drives a relatively fast plastic strain recovery observed experimentally as the transient plastic strain recovery rate. After the diffusive mechanisms have removed the excess material in the diffusion zone near the void tip, the rate of diffusion slows to that due to the difference between the chemical potential on the grain boundary and the chemical potential on the void surface. This slower diffusion flux is interpreted experimentally as the steady state plastic strain recovery rate.

Our numerical simulations capture the experimentally observed plastic strain recovery both qualitatively and quantitatively. Specifically, Fig. 11a shows the plastic strain recovery as a function of time and Fig. 11b shows the evolution of the normal stress on the grain boundary near the void tip as a function of time on the grain boundary throughout the plastic strain recovery

Conclusions

We characterized plastic strain recovery and creep in free-standing nanocrystalline copper films with thickness of couple of hundreds of nanometers. The plane-strain bulge test was performed to measure the material properties such as Young's Modulus and creep strain rate. The Young's modulus obtained is in the range suggested in literature for copper. Based on the strain rate during creep and using Coble creep equation, the atomic diffusion flux was obtained. It was very close to the value suggested with other groups work through numerical simulation for nanocrystalline materials. The experimental results shows that plastic strain recovery occurs when the loading rate is in the order of or less than $10^{-6}/s$. The recovery occurs in two rates for the test at room temperature as well as at $100\,^{\circ}C$. The initial transient rate is is relative fast followed by a slower steady state rate. The second recovery rate is in the order of $10^{-9}/s$ regardless of the deposition method, temperature, and loading rate, and the first rate is around $10^{-7}/s$ and $10^{-8}/s$ for loading rates of $10^{-6}/s$ and $10^{-7}/s$ respectively. These rates do not depend on deposition method and temperatures well below the melting point. A diffusive mechanism involving grain reversing flux between grain boundaries and void surfaces is proposed as being responsible for plastic strain recovery.

Acknowledgments The authors gratefully acknowledge support from the National Science Foundation (NSF DMR-1310503).

References

1. Hall EO (1951) The deformation and ageing of mild steel: Iii discussion of results. Proc Phys Soc 64(32)
2. Petch NJ (1953) The cleavage strength of polycrystals. J Iron Steel Inst:173
3. Gleiter H. (1989) Nanocrystalline materials. Progress Mater Sci 33(4):223–315
4. Gleiter H (2000) Nanostructured materials: basic concepts and microstructure. Acta Materialia 48(1):1–29
5. Kumar KS, Swygenhoven HV, Suresh S (2003) Mechanical behavior of nanocrystalline metals and alloys. Acta Materialia 51(19):5743–5774. The Golden Jubilee Issue. Selected topics in Materials Science and Engineering: Past, Present and Future
6. Weertman JR (2007) Nanostructured materials: processing, properties and applications, 2nd edn. William Andrew Inc, NY, p 537
7. Wei X, Kysar JW (2011) Residual plastic strain recovery driven by grain boundary diffusion in nanocrystalline thin films. Acta Materialia 59(10):3937–3945
8. Rajagopalan J, Han JH, Saif MTA (2007) Plastic deformation recovery in freestanding nanocrystalline aluminum and gold thin films. Science 315(5820):1831–1834
9. Meyers MA, Mishra A, Benson DJ (2006) Mechanical properties of nanocrystalline materials. Progress Mater Sci 51(4):427–556
10. Wei Y, Bower AF, Gao H (2008) Recoverable creep deformation and transient local stress concentration due to heterogeneous grain-boundary diffusion and sliding in polycrystalline solids. J Mech Phys Solids 56(4):1460–1483
11. Swygenhoven HV, Derlet PM (2001) Grain-boundary sliding in nanocrystalline fcc metals. Phys. Rev. B 64(9):224105
12. Wei YJ, Anand L (2004) Grain-boundary sliding and separation in polycrystalline metals: application to nanocrystalline fcc metals. J Mech Phys Solids 52(11):2587–2616
13. Keblinski P, Wolf D, Gleiter H (1998) Molecular-dynamics simulation of grain-boundary diffusion creep. Inter Sci 6:205–212
14. Schiotz J, Di Tolla FD, Jacobsen KW (1998) Softening of nanocrystalline metals at very small grain sizes. Nature 391(6667):561–563, 02
15. Conrad H, Narayan J (2000) On the grain size softening in nanocrystalline materials. Scripta Materialia 42(11):1025–1030, 5
16. Wolf D, Yamakov V, Phillpot SR, Mukherjee AK (2003) Deformation mechanism and inverse hall–petch behavior in nanocrystalline materials. Zeitschrift für Metallkunde 94(10):1091–1097, 2015/04/27
17. Wei Q, Cheng S, Ramesh KT, Ma E (2004) Effect of nanocrystalline and ultrafine grain sizes on the strain rate sensitivity and activation volume: fcc versus bcc metals. Mater Sci Eng A 381:71–79

18. Wei Y, Bower AF, Gao H (2008) Enhanced strain-rate sensitivity in fcc nanocrystals due to grain-boundary diffusion and sliding. Acta Materialia 56(8):1741–1752
19. Arzt E (1998) Size effects in materials due to microstructural and dimensional constraints: a comparative review. Acta Materialia 46(16):5611–5626
20. Gad el Hak M (2001) The MEMS Handbook. CRC Press
21. Bhushan B, Li X (2003) Nanomechanical characterisation of solid surfaces and thin films. Int Mater Rev 48(3):125–164
22. Oliver WC, Pharr GM (2004) Measurement of hardness and elastic modulus by instrumented indentation: advances in understanding and refinements to methodology. J Mater Res 19:3–20, 1
23. Chen X, Vlassak JJlassak JJ (2001) Numerical study on the measurement of thin film mechanical properties by means of nanoindentation. J Mater Res 16:2974–2982, 10
24. Tsui TY, Vlassak JJ, Nix WD (1999) Indentation plastic displacement field: Part i. the case of soft films on hard substrates. J Mater Res 14:2196–2203, 6
25. Hong S, Weihs TP (1989) Residual stresses in thin film using microcantilever beams in thin films. Stress Mech Prop 130:93–98
26. Baker SP, Nix WD (1994) Mechanical properties of compositionally modulated au-ni thin films: nanoindentation and microcantilever deflection experiments. J Mater Res 9:3131–3144, 12
27. Baker SP, Keller-Flaig RM, Shu JB (2003) Bauschinger effect and anomalous thermomechanical deformation induced by oxygen in passivated thin cu films on substrates. Acta Materialia 51(10):3019–3036
28. Xiang Y, Chen X, Vlassak JJ (2005) Plane-strain bulge test for thin films. J Mater Res 20:2360–2370, 9
29. Han SW, Lee HW, Lee HJ, Kim JY, Kim JH, Oh CS, Choa SH (2006) Mechanical properties of au thin film for application in mems/nens using microtensile test. Curr Appl Phys 6, Supplement 1(0):e81 – e85. Nano Korea 2005 Symposium Nano Korea 2005 Symposium
30. Freund LB, Suresh S (2003) Thin film materials: stress, defect formation, and surface evolution. Cambridge University Press, New York
31. Zhou W, Yang J, Sun G, Liu X, Fuhua Y, Jinmin L (2008) Fracture properties of silicon carbide thin films by bulge test of long rectangular membrane. J Microelectromech Syst 17(2):453–461
32. Tugcu P, Neale KW, Wu PD, Inal K (2004) Crystal plasticity simulation of the hydrostatic bulge test. Int J Plastic 20:1603–1653
33. Gruber PA, Böhm J, Onuseit F, Wanner A, Spolenak Rcand Arzt E (2008) Size effects on yield strength and strain hardening for ultra-thin cu films with and without passivation: a study by synchrotron and bulge test techniques. Acta Materialia 56(10):2318–2335
34. Huang CK, Lou WM, Tsai CJ, Wu TC, Lin HY (2007) Mechanical properties of polymer thin film measured by the bulge test. Thin Solid Films 515(18):7222–7226
35. Vlassak JJ, Nix WD (1992) A new bulge test technique for the determination of young's modulus and poisson's ratio of thin films. J Mater Res 7(12):3242–3249
36. Xiang Y, Chen X, Vlassak JJ (2005) Plane-strain bulge test for thin films. J Mater Res 20(9):2360–2370
37. Vlassak JJ, Nix WD (1992) A new bulge test technique for the determination of young's modulus and poisson's ratio of thin films. J Mater Res 7:3242–3249, 12
38. Wei X, Lee D, Shim S, Chen X, Kysar JW (2007) Plane-strain bulge test for nanocrystalline copper thin films. Scripta Materialia 57(6):541–544
39. Yong X, Tsui TY, Vlassak JJ, McKerrow AJ (2004) Measuring the elastic modulus and ultimate strength of low-k dielectric materials by means of the bulge test:133
40. Zhou W, Yang J, Li Y, Ji A, Yang F, Yu Y (2009) Bulge testing and fracture properties of plasma-enhanced chemical vapor deposited silicon nitride thin films. Thin Solid Films 517(6):1989–1994
41. Xiang Y, Tsui TY, Vlassak JJ (2006) The mechanical properties of freestanding electroplated cu thin films. J Mater Res 21:1607–1618, 6
42. Hencky H (1915) About the stress state in circular plates with negligible bending stiffness. Math Phys 63(311)
43. Vlassak JJ (1994) New experimental techniques and analysis methods for study of mechanical properties of materials in small volumes. PhD thesis, Stanford University, Stanford, CA
44. Tabata O, Kawahata K, Sugiyama S, Igarashi I (1989) Mechanical property measurments of thin films using load-deflection of composite rectangular membrane. In: Proceeding, micro electro mechanical systems IEEE, pp 152–156
45. Lin P (1990) The in-situ measurement od mechanical properties of multi-layer coatings. PhD thesis, Massachusetts Institue of Technology, Cambridge, MA
46. Timoshenko S, Woinowsky-Krieger S (1959) Theory of plates and shells. McGraw-Hill, New York
47. Maseeh F, Senturia SD (1990) Viscoelasticity and creep recovery of polyimide thin films. IEEE Solid-State Sensor Actuator Workshop:55
48. Kelly PJ, Arnell RD (1999) Control of the structure and properties of aluminum oxide coatings deposited by pulsed magnetron sputtering. J Vacuum Sci Technol 17:945
49. Kelly PJ, Arnell RD (2000) Magnetron sputtering: a review of recent developments and applications. Vacuum 56(3):159–172
50. Scherrer P (1918) Estimation of the size and internal structure of colloidal particles by mean of rontgen. Nachr GEs Wiss Gottingen 2:96–100
51. Williamson GK, Hall WH (1953) X-ray line broadening from filed aluminium and wolfram. Acta Metallurgica 1(1):22–31
52. Cullity BD (2001) Elements of x-ray diffraction, 3rd edn. Prentice Hall, Upper Saddle River
53. Warren BE, Averbach BL (1950) The effect of cold-work distortion on x-ray patterns. J Appl Phys 21(595)
54. Sanchez-Bajo F, Cumbrera FL (1997) The use of the pseudo-voigt function in the variance method of x-ray line-broadening analysis. J Appl Cryst 30:427–430
55. Standard test methods for determining average grain size. *ASTM International* (2013)
56. International A. Metals Handbook:. ASM International, Materials Park, Ohio (1990)
57. Fougere GE, Riester L, Ferber M, Weertman JR, Siegel RW (1995) Young's modulus of nanocrystalline Fe measured by nanoindentation. Mater Sci Eng A-Struct Mater Prop Microstruct Process 204(1–2):1–6. Symposium on Engineering of Nanostructured Materials, BOSTON, MA, NOV 28-30, 1994
58. Coble RL (1963) A model for boundary diffsuion controlled creep in polycrystalline materials. J Appl Phys 34:1679–1682
59. Yamakov V, Wolf D, Phillpot SR, Gleiter H (2002) Grain-boundary diffusion creep in nanocrystalline palladium by molecular-dynamics simulation. Acta Materialia 50(1):61–73
60. Karch J, Birringer R, Gleiter H (1987) Ceramics ductile at low temperature. Nature 330(6148):556–558, 12
61. Nieman GW, Weertman JR, Siegel RW (1991) Mechanical behavior of nanocrystalline cu and pd. J Mater Res 6(5):1012–1027
62. Hugo RC, Kung H, Weertman JR, Mitra R, Knapp JA, Follstaedt DM (2003) In-situ tem tensile testing of dc magnetron sputtered and pulsed laser deposited ni thin films. Acta Materialia 51:1937–1943